Supporting Information

Nickel Nitride-Black Phosphorus Heterostructure Nanosheets for Boosting Electrocatalytic Activity towards Oxygen Evolution

Tong Wu[a,b,c] ,Shaoning Zhang[a] ,Kejun Bu[a,b] ,Wei Zhao[a] ,Qingyuan Bi[a] ,Tianquan Lin [a,*] ,Jian Huang[a] ,Yongsheng Li[c,*] and Fuqiang Huang[a,d,*]

[a]State Key Laboratory of High Performance Ceramics and Superfine Microstructure, Shanghai Institute of Ceramics, Chinese Academy of Sciences, Shanghai 200050, P. R. China

[b]University of Chinese Academy of Sciences, Beijing, 100049, P. R. China

[c]Lab of Low-Dimensional Materials Chemistry, Key Laboratory for Ultrafine Materials of Ministry of Education, School of Materials Science and Engineering, East China University of Science and Technology, Shanghai 200237, P. R. China

[d]State Key Laboratory of Rare Earth Materials Chemistry and Applications, College of Chemistry and Molecular Engineering, Peking University, Beijing 100871, P. R. China

Corresponding Authors

E-mail: huangfq@mail.sic.ac.cn; ysli@ecust.edu.cn; lintianquan@mail.sic.ac.cn

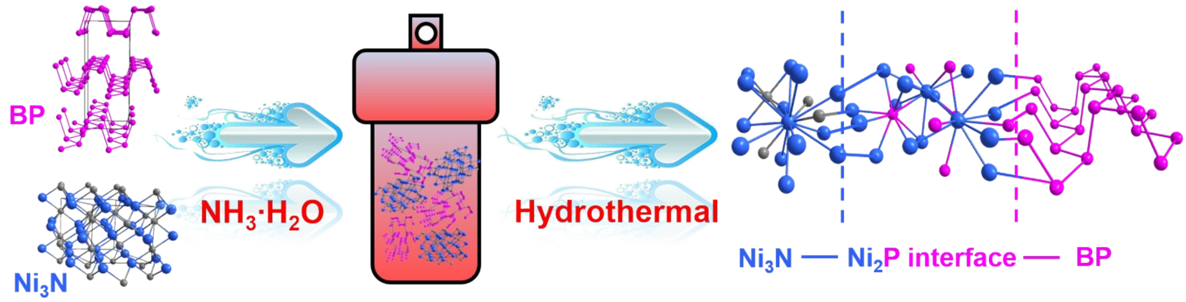

Fig. S1. Illustration of the fabrication and catalytic processes of <Ni_3N|Ni_2P|BP> nanosheets.

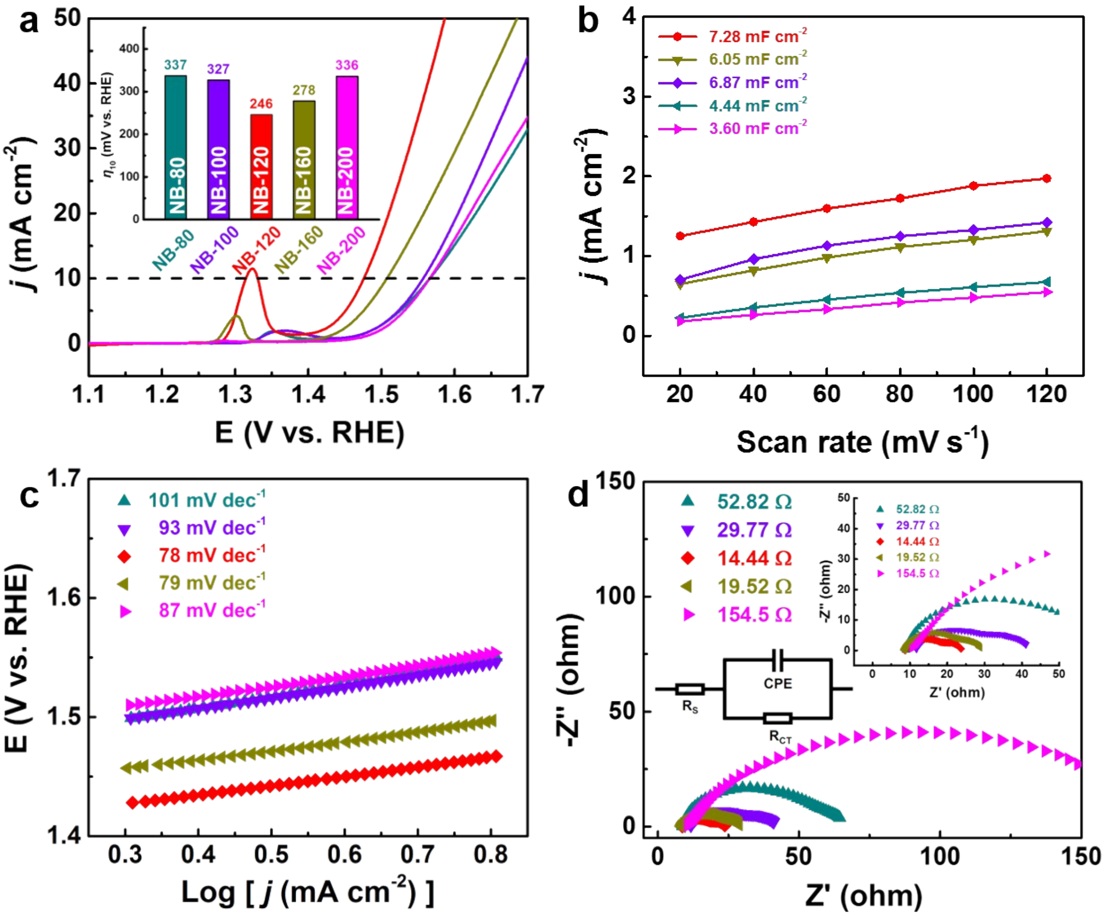

Fig. S2. (a) LSV curves (Inset: overpotentials required for j = 10 mA cm^{-2}), (b) Plots used to extract the double-layer capacitances (C_{dl}) and estimate the relative electrochemically active surface areas, (c) Tafel plots and (d) Nyquist plots of NB-80, NB-100, NB-120, NB-160, and NB-200, respectively.

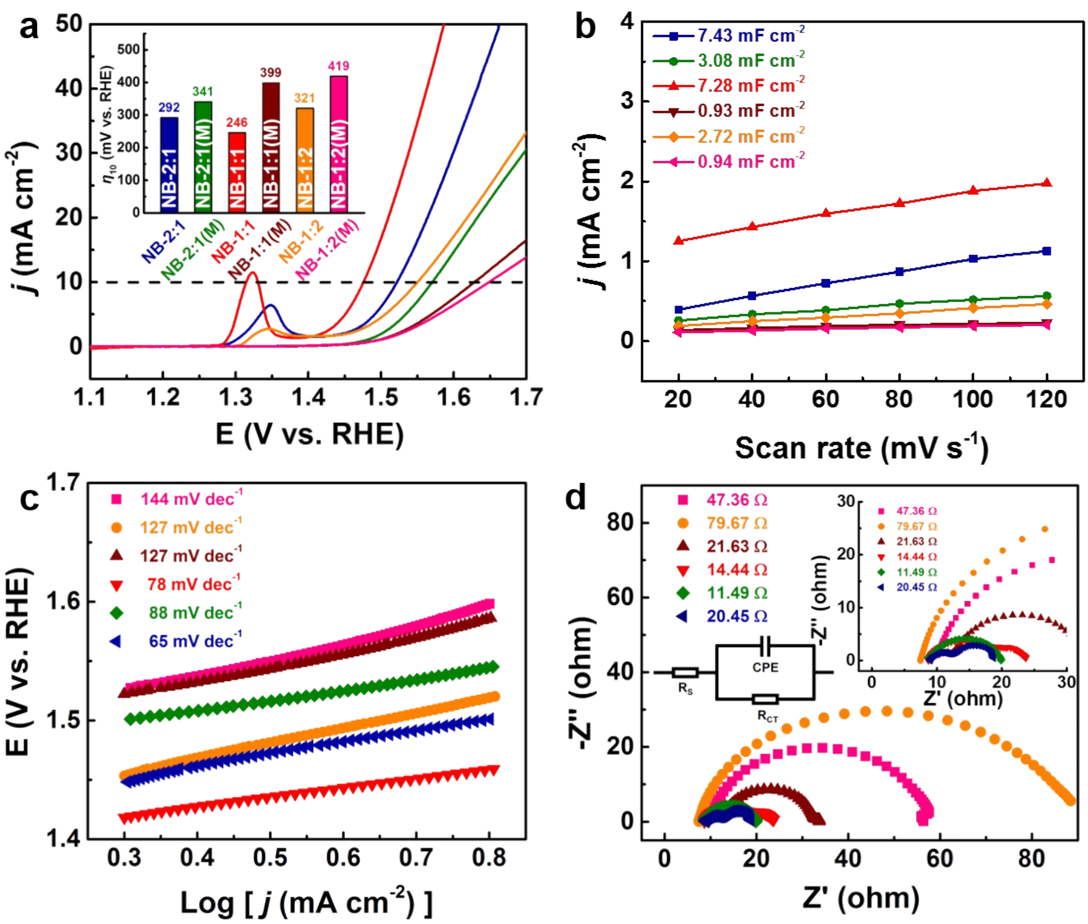

Fig. S3. (a) LSV curves (Inset: overpotentials required for j = 10 mA cm^{-2}), (b) Plots used to extract the double-layer capacitances (C_{dl}) and estimate the relative electrochemically active surface areas, (c) Tafel plots and (d) Nyquist plots of NB-2:1, NB-2:1(M), NB-1:1, NB-1:1(M), NB-1:2, and NB-1:2(M), respectively.

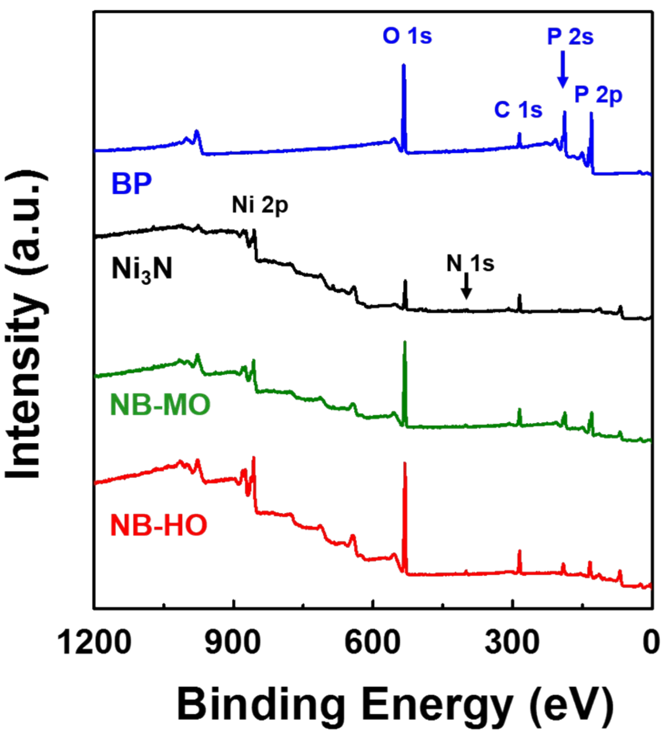

Fig. S4. The XPS survey spectra of BP, Ni_3N, NB-MO, and NB-HO, respectively.

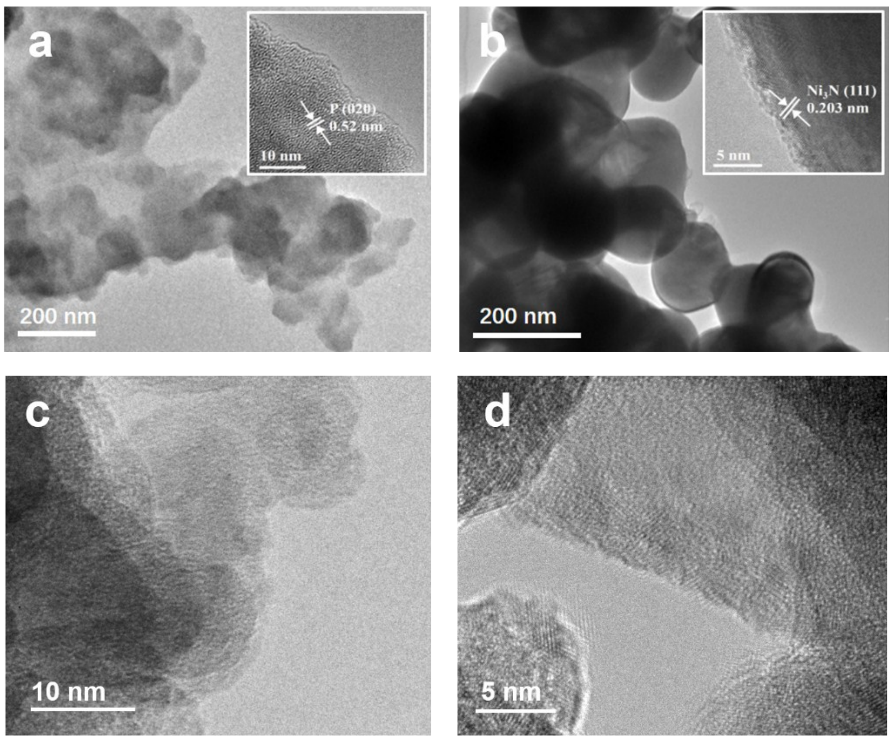

Fig. S5. TEM images of (a) BP (Inset: corresponding HRTEM image), (b) Ni_3N (Inset: corresponding HRTEM image), (c) TEM image of NB-HO nanosheets, (d) HRTEM image of NB-HO nanosheets.

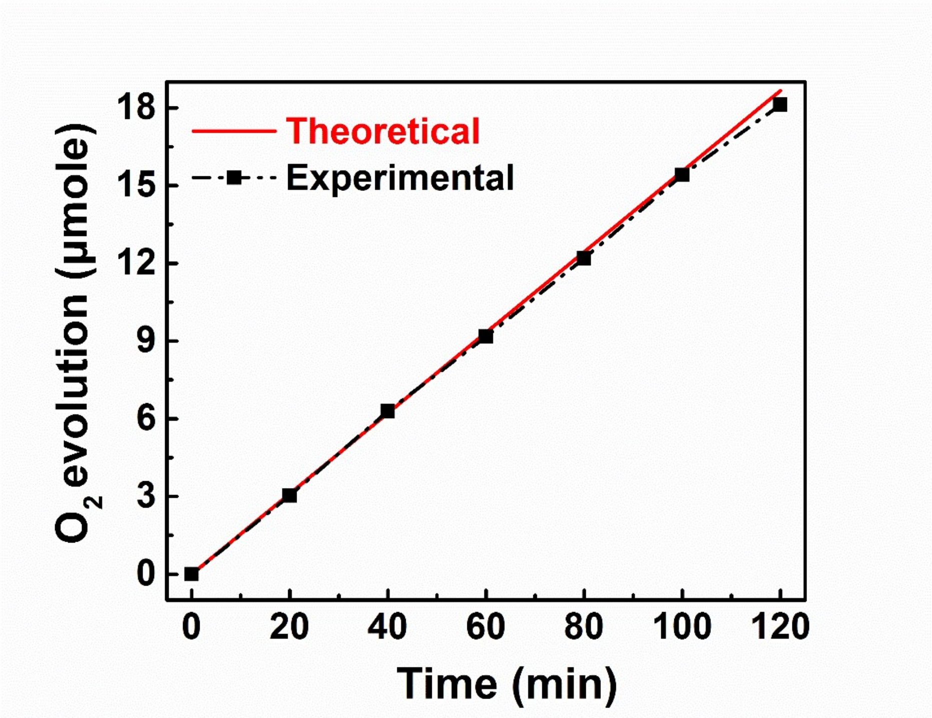

Fig. S6. The experimental and theoretical O_2 evolution amount of NB-OH electrode at a constant oxidative current of 1 mA. Clearly the Faradaic efficiency of NB-OH electrode for water oxidation is over 98%.

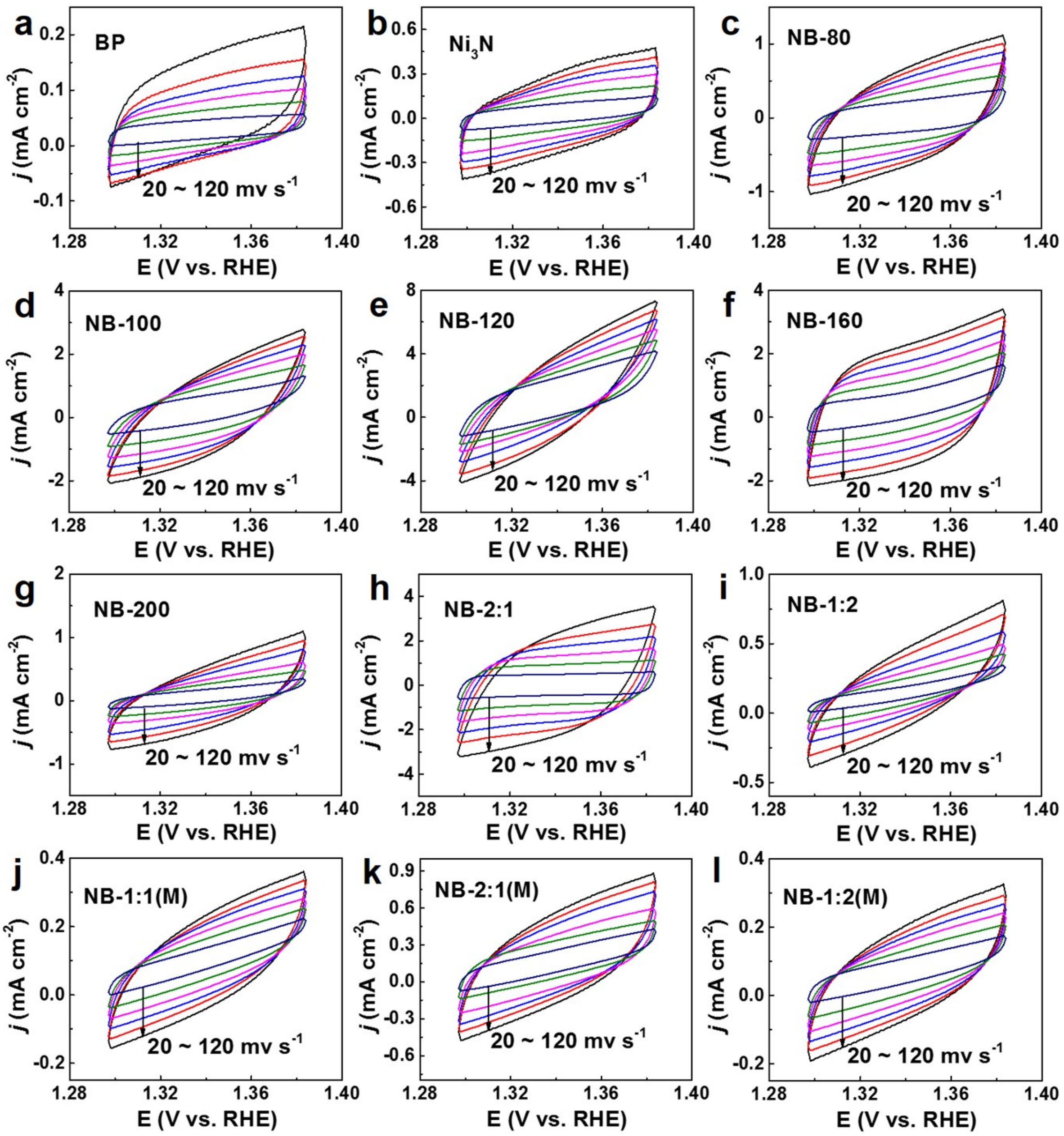

Fig. S7. Cyclic voltammetry (CV) curves of (a) BP, (b) Ni_3N, (c) NB-80, (d) NB-100, (e) NB-120, (f) NB-160, (g) NB-200, (h) NB-2:1, (i) NB-1:2, (j) NB-1:1(M), (k) NB-2:1(M) and (l) NB-1:2(M) measured under the potential window of 1.297-1.383 V vs. RHE with different scan rate from 20 to 120 mV/s.

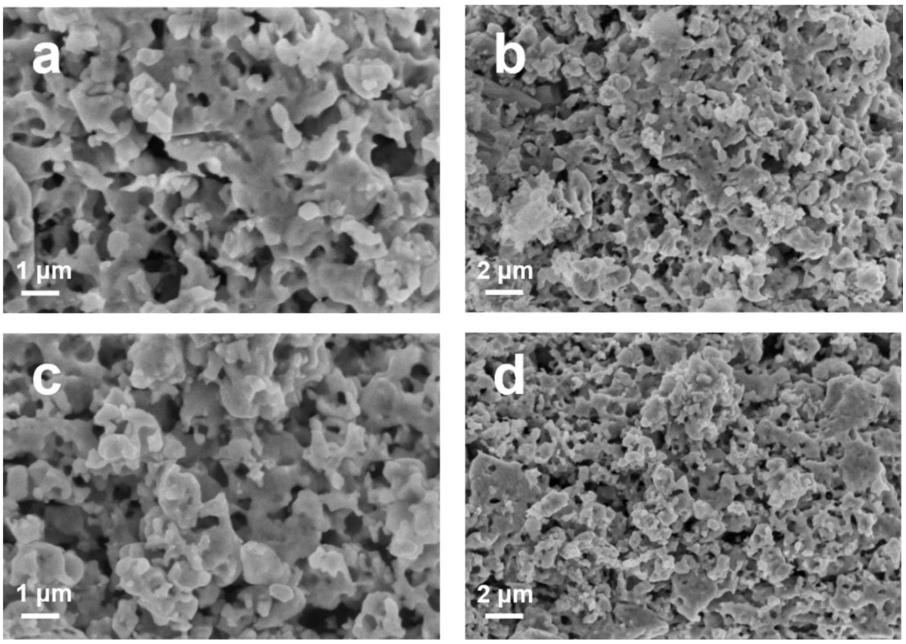

Fig. S8. SEM images of NB-HO (a, b) before and (c, d) after OER.

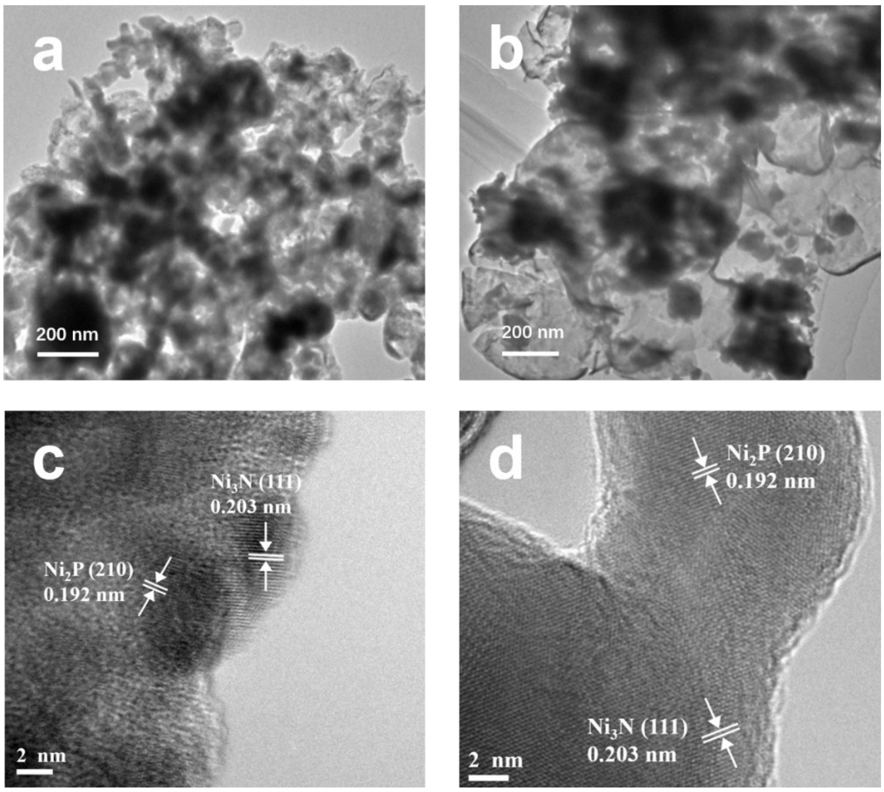

Fig. S9. TEM images of NB-HO (a) before and (b) after OER. HRTEM images of NB-HO (c) before and (d) after OER.

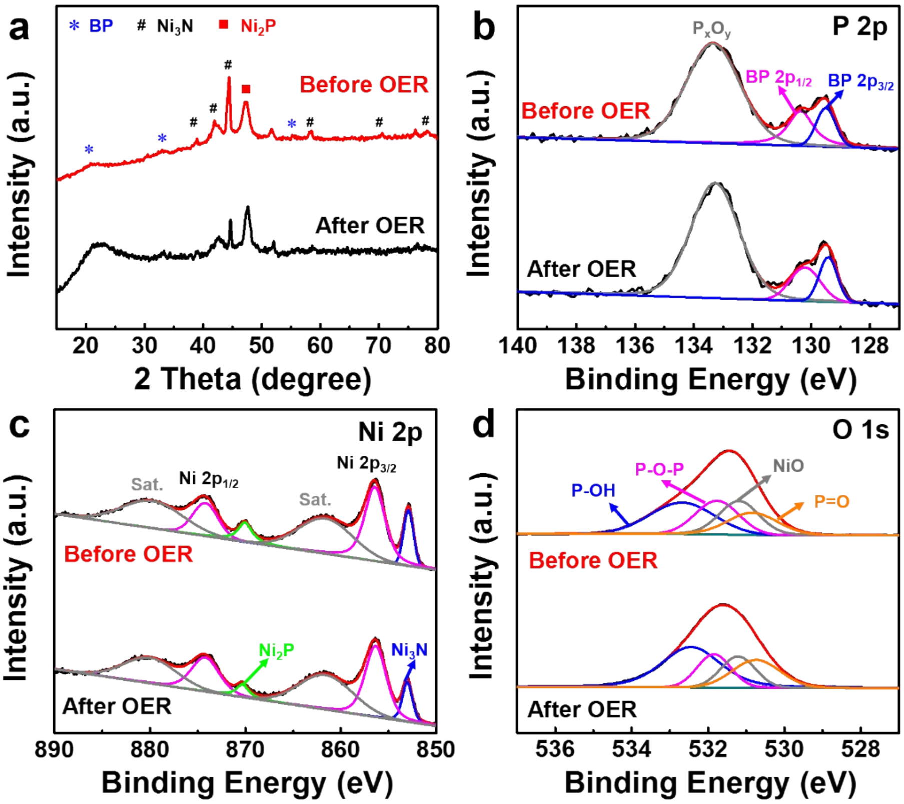

Fig. S10. (a) XRD patterns of NB-HO before and after OER. (b) High-resolution P 2p XPS spectra of BP, NB-MO, and NB-HO. (c) High-resolution Ni 2p XPS spectra of Ni3N, NB-MO, and NB-HO. (d) High-resolution O 1s XPS spectra of BP, Ni3N, NB-MO, and NB-HO.

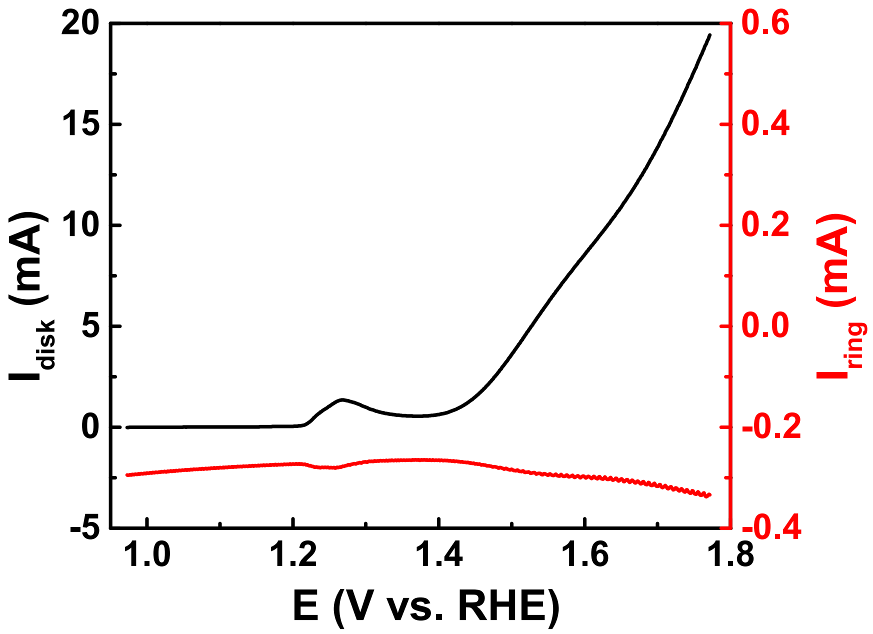

Fig. S11. Ring and disk currents for the NB-OH on Rotating ring-disk electrode (RRDE) in 1 M KOH supporting electrolyte. E_{Ring} = 0.4 V vs RHE. The n value can be calculated from the disk current (id) and ring current (ir) using eq1: $n = 4 \times \frac{i_d}{i_d + \frac{i_r}{N_c}}$ (1). where N_C is the collection efficiency of the RRDE, defined as the fraction of product from the disk to the ring.

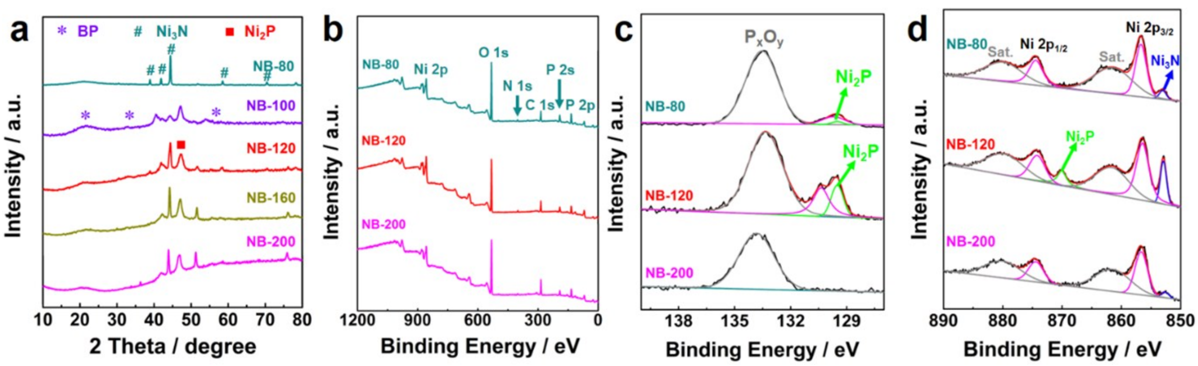

Fig. S12. (a) XRD patterns of NB-80, NB-100, NB-120, NB-160, and NB-200, respectively. (b) XPS survey spectra, (c) High-resolution P 2*p* XPS spectra, and (d) High-resolution Ni 2*p* XPS spectra of NB-80, NB-120 and NB-200.

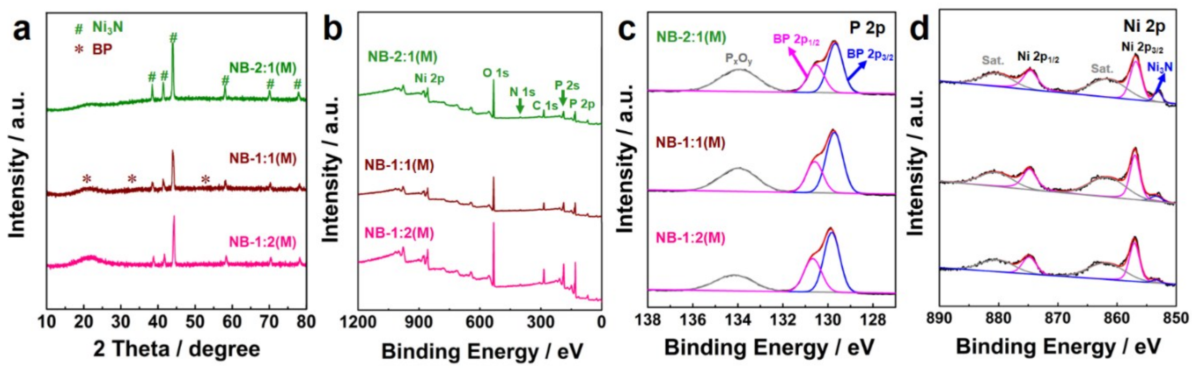

Fig. S13. (a) XRD patterns, (b) XPS survey spectra, (c) High-resolution P 2*p* XPS spectra, and (d) High-resolution Ni 2*p* XPS spectra of NB-2:1(M), NB-1:1(M), and NB-1:2(M).

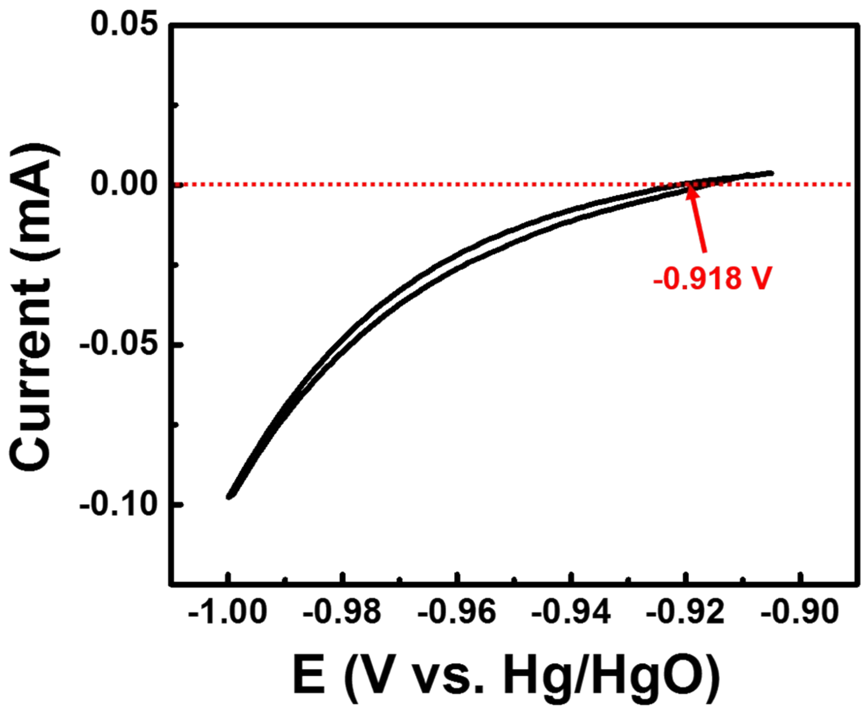

Fig. S14. The calibration curves for reference electrode in 1 M KOH supporting electrolyte.

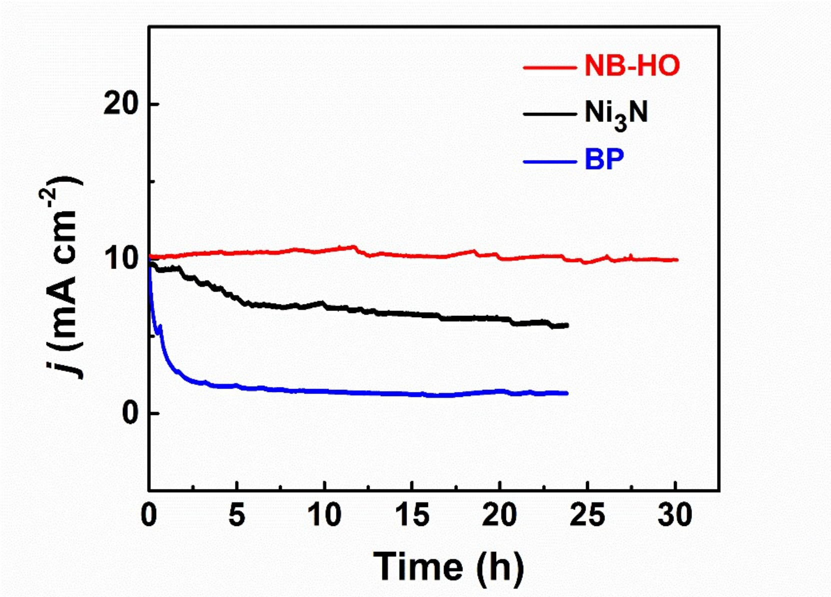

Fig. S15. Chronoamperometry curves of NB-HO, Ni3N, and BP at overpotentials of 246, 340, and 451 mV, respectively.

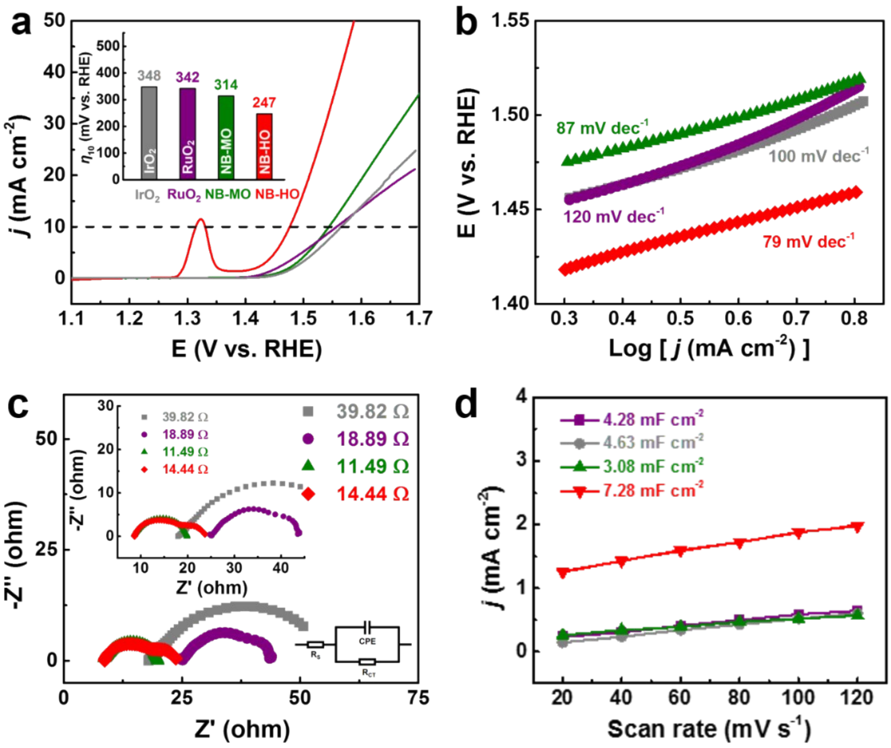

Fig. S16. (a) LSV curves of IrO_2, RuO_2, NB-MO, and NB-HO (Inset: overpotentials required for j = 10 mA cm^{-2}). (b) Tafel plots of IrO_2, RuO_2, NB-MO, and NB-HO, respectively. (c) Nyquist plots of IrO_2, RuO_2, NB-MO, and NB-HO, respectively. (d) Plots used to extract the double-layer capacitances (C_{dl}) and estimate the relative electrochemically active surface areas.

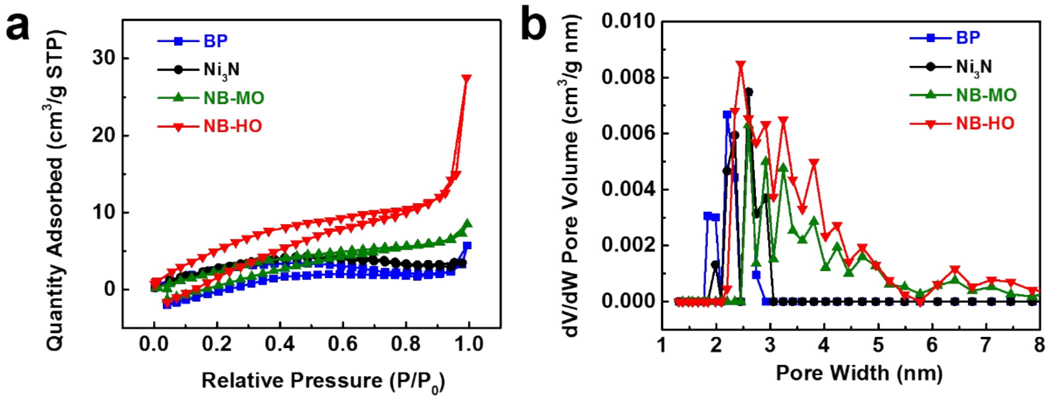

Fig. S17. (a) Nitrogen adsorption/desorption isotherms of BP, Ni_3N, NB-MO, and NB-HO and (b) Barret-Joyner-Halenda (BJH) pore size distributions for BP, Ni_3N, NB-MO, and NB-HO.

Table S1. Comparison of the OER activities of the NB-HO with some recently-reported OER catalysts.

Catalysts	η_{10} (mV)	Tafel slope (mV dec^{-1})	Loading mass (mg cm^{-2})	Substrate	Ref.
NB-HO	**247**	**79**	**0.25**	**GC**	**This Work**
Mn_3N_2	270	101	3.0	NF	Ref. 5
^{s}Au/NiFe LDH	237	36	2.0	Ti mesh	Ref. 36
NiFeCr LDH	280	131	0.2	GC	Ref. 37
Boronized Ni plate	300	47	Not reported	Boronized Ni plate	Ref. 38
Ni-Fe LDH hollow nanoprisms	280	49.4	0.16	GC	Ref. 39
MoO_x@N3-doped MoS_{2-x}	270	61	0.36	GC	Ref. 40
MnCoP nanoparticles	330	61	0.284	GC	Ref. 41
$CoFeP_x$	323	58	Not reported	GC	Ref. 42
$Fe_{0.33}Co_{0.67}OOH$ PNSAs	266	30	1.394	CFC	Ref. 43
NiV LDH	318	50	0.143	GC	Ref. 44
G-FeCoW	223	37	0.21	GC	Ref. 45
Co-PBA-plasma 2 h	274	53	2.0	Ni foam	Ref. 46
CoO-S	326	63.9	0.16	GC	Ref. 47
SnCoFe-Ar	300	42.3	Not reported	GC	Ref. 48
Ni_2P/Ni/NF	260	72	Not reported	NF	Ref. 17
$Mg_2Ni_{12}P_7$	280	48	1.3	C paper	Ref. 49
$Ni_{1.25}Ru_{0.75}P$	340	Not reported	0.284	GC	Ref. 50
Ni-Co-P HNBs	270	76	2.0	NF	Ref. 51
NF@Ni/C-600	265	57	7.3	NF	Ref. 52

Electrolyte: 1 M KOH